2022

Analysis of Droplet Motion – Sliding On and Detaching From a Vertical Surface

Haoyang Zou

Hongqing Jin

Sophie Wang

Analysis of droplet motion - sliding on and detaching from a vertical surface

Haoyang ZOU[1], Hongqing JIN[1], Sophie WANG[1*]

[1] Mechanical Science and Engineering, University of Illinois at Urbana-Champaign
Urbana, IL, 61801, USA
(+1 217-265-9232, wangxf@illinois.edu)

* Corresponding Author

ABSTRACT

Droplets sliding on and detaching from a surface exist in all different scenarios, and this motion is essential since retention and shedding of droplets affect energy consumption and system performance in many applications, for example air dehumidification and heat pump systems. While multiple factors affect the droplet motion, including droplet size, surface energy and micro-nano structure, air velocity etc., there is few good models to predict the motion of droplet, especially how the droplet overcomes the pin of the surface edge. In this work, experiment has been conducted to investigate droplet motions while it is sliding down different surfaces. Droplet velocity, dynamic contact angle (receding and advancing) has been measured through image processing. Force analysis is conducted for different stages of droplet motion down the vertical surface, and together with experiment data, impacts of various factors including droplet shape variation have been identified and qualitatively analyzed. Additionally, hydrophilic-hydrophobic wettability gradient is introduced to the scenario. It is found that length of the hydrophobic coating region has an impact on its improvement of water drainage. The results derived from this work provide a deeper understanding of droplet motion on surfaces under gravitational force and can serve as the guidance for heat exchanger design.

1. INTRODUCTION

Droplet retention and detachment are very important subjects in air conditioning and refrigeration. In air-cooling and dehumidification systems, condensed water accumulates on air-side surfaces of the heat exchanger, and amount of retained water on such surfaces depends upon droplet detachment. In some heat pump systems, drainage of water droplets is also required during defrosting process of such systems. Droplet detachment is also ubiquitous in many civil and industrial applications. This includes modelling ice accretion on wires during freezing rain (Makkonen, 1984), spray cooling and painting (Hung and Yao, 1999), coalescer used in fluid separation or fog harvesting (Wang and Desjardins, 2018).

Previous research on heat exchangers has proved the importance of water drainage by revealing impact of retained water on thermal and hydraulic performances. Tang and Jacobi (2001) showed that in louvered fin heat exchangers, wet airside heat transfer coefficient can be 10% to 100% lower than on the dry airside, and friction factor of wet airside is also notably higher, with an increase from 10% to 70% over dry condition. In search of practical method to mitigate airside condensate retention, researchers made various attempts to model water retention on plain fin and other fin structures, hence finding the better option among different kinds of fin surfaces and reasons behind their performances. Min and Webb (2001) established experimental method for observing and studying water drainage on vertical fin surfaces, and tested drainage performance on different surfaces materials, with a variety of surface treatments. It was found that surface wettability plays a key role in retained condensate mass on the vertical fins, and condensate mass per unit area is a function of receding contact angle of water on the surface. However, only qualitative trend was obtained from these experiments, while little physics in droplet retention was discussed. Another approach from Korte and Jacobi (1997) started by modelling maximum diameter for single retained droplet using force balance and getting relationship between retained droplet volume and drop diameter. With maximum retained droplet volume and a droplet size distribution model, a reasonable success was achieved in predicting condensate retention on plain fins with wide fin spacing. However, simplification through assumptions in droplet shape limited applicability of the model. Later this approach was improved by ElSherbini (2003), ElSherbini and Jacobi (2004, I), ElSherbini and Jacobi (2004, II),

ElSherbini and Jacobi (2006) and better models were obtained, but limitation in droplet shape approximation still exists.

The existing works on water retention only consider droplet retention in midst of vertical or inclined surface but did not take the droplet pinning phenomenon at either fin bottom edge (vertical) or trailing edge into account. As shown in experiment results in this work, maximum retained droplet volume can be approximately twice as much as the critical volume for droplet to start sliding. Thus, droplet pinning can lead to considerable inaccuracy in existing condensate retention models. Also, in some other applications such as predicting water bridging, inaccurate estimation of retained droplet volume can be a big issue. Since sliding droplet can still retain at trailing edge, dynamic wetting during sliding and droplet behavior after pinning are worth focusing on. However, very little work has been focusing on these topics. Kim *et al.* (2001) constructed a scaling law that explained dependence of droplet sliding velocity on various parameters of the smooth surface, but this work only discussed the case where droplet is at its stable sliding velocity, without considering droplet accelerating process when sliding distance is limited. Wang *et al.* (2016) examined the process of droplet sliding down and encountering wettability gradient, where similar pinning phenomenon is present.

In this work, droplet sliding on a vertical surface was observed with focus on droplet pinning at the surface edge or the boundary of wettability. Different stages during the sliding process were discussed, force balance based analysis was established to predict the criteria of the pining, oscillation and detaching of the droplet.

2. EXPERIMENTAL METHODS

2.1 Experiment Procedures

The experimental apparatus is shown in figure 1, which includes a micro syringe pump, a syringe, a tube, a needle, a rotatable stand, an LED light source, a high-speed camera, and sample surface to be tested.

Before starting an experiment, the rotatable stand is first adjusted to the orientation to be tested. Then screws are used to assemble the sample surface to rotatable stand and ensure the sample to remain flat. Depending on the tested droplet volume, needle with proper gage is selected.

During the experiment, the micro syringe pump pumps out water of specific volume. The water goes through the tube and departs from needle, thus forming a droplet at the marked starting position on the sample surface. The high-speed camera is used to record droplet motion until it detaches from, or stops on the sample surface, at a rate of 1000 frames per second.

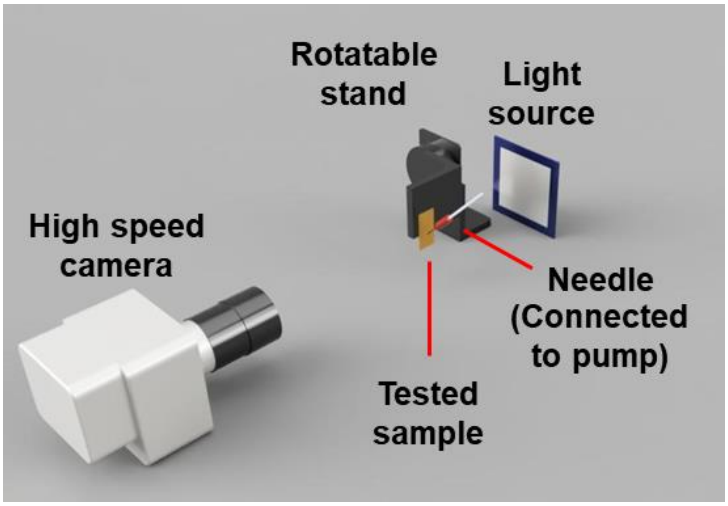

Figure 1. Schematic of experimental apparatus for the measurements of droplet motion and dynamic contact angles

2.2 Experiment Conditions

Experiment conditions are shown in Table 1. Since aluminum is one of the most common materials in heat exchanger designs, Aluminum 6061 is being used in experiments. Sample are cut into a dimension of 25.4 mm×50.8 mm×0.635 mm. On each tested sample, a starting mark is made at a specific distance from sample edge, and the droplet lower

bound will be aligned with starting mark at the beginning of each trial. In this work, droplet initial position is set to 10 mm from sample edge, which is an estimation for droplet sliding distance on heat exchangers. Partially hydrophobic coated aluminum samples are being tested in experiments, and each of these samples are being coated for a specific length (see figure 2) with water repellant spray, thus creating a wettability gradient on the sample. The static and dynamic contact angles for sample surfaces are measured and listed in Table 2.

Table 1: Experiment conditions

Surface	v_{air}	Sliding distance	Orientation
Uncoated Partially hydrophobic coated (L_{coat} =1, 2, 5 mm)	0 m/s	10 mm	90° (vertical)

Table 2. Static and dynamic contact angle for sample surfaces

Surface	θ_{static}	θ_{ad}	θ_{re}
Uncoated	83.4°	93.4°	17.6°
Hydrophobic coated	124.7°	146.3°	48.5°

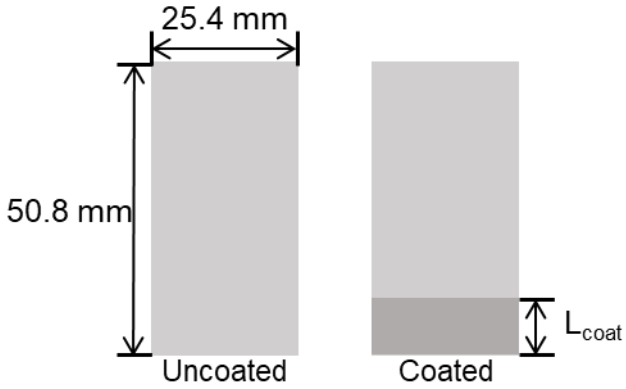

Figure 2. Sample surface configurations

2.2 Measurement Method

Image processing codes (Python) is used to batch process images obtained from experiment videos. Functions of the codes include: (1) Polarize images and remove noise; (2) Mask images with dry sample image, leaving only droplet on the image; (3) Capture specific point on the droplet and record y-positions; (4) Measure dynamic contact angles at the front and the back of droplet.

Accuracy of all measurements made in the image processing code is limited by the image resolution. For position measurements involved in this work, the code resolves lengths with an accuracy of 1 pixel, which is 33.421 μm. Contact angle measurements in this work is realized by polynomial fitting to droplet profile. Through repeat testing, the uncertainty of angle measurements is estimated to be 2.8°.

When capturing droplet positions, the image processing code has 3 options in its output: lowest point, advancing contact line, centroid, as indicated in figure 3 (a). In this work, droplet positions are obtained from centroid. To validate usage of this information and estimate uncertainty from this measurement, the result is compared with results from measuring other points:

In the position plot, the difference between measured values indicates that the 3 points are found at different y-positions, while no major difference in their motion is found. In velocity plot, advancing contact line velocity shows smaller magnitude compared to the other two position results, especially during the droplet oscillation process. This discrepancy is due to droplet pinning at either sample edge or the wettability gradient, which also makes advancing contact line position less representative to the droplet motion during oscillation. Comparing centroid and lowest point results on velocity plot, only small difference of about 4 mm/s at max is identified. Considering the significance of center of mass in droplet motion analysis, centroid is the better option among available outputs of the code.

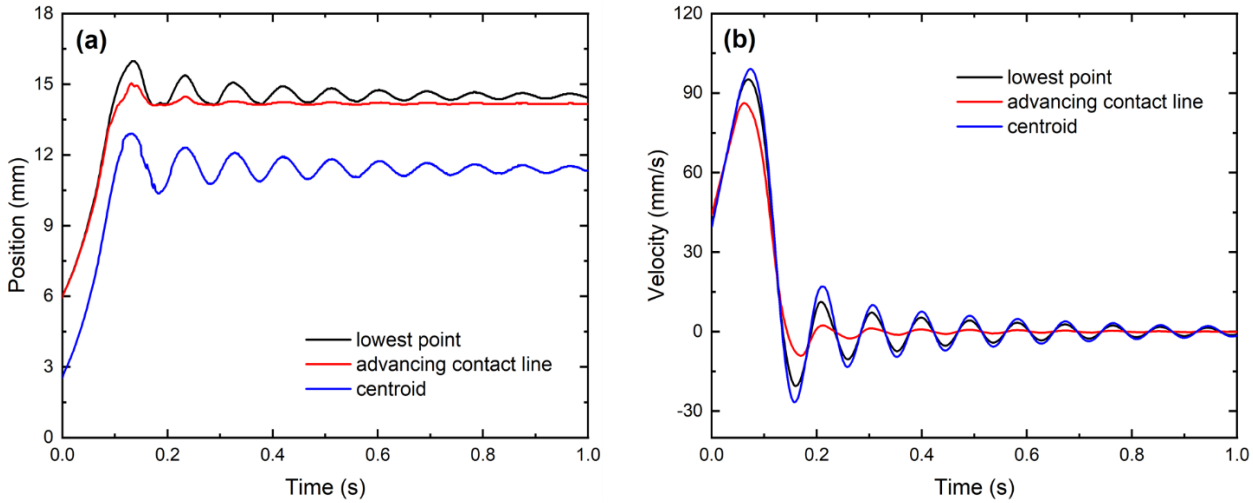

Figure 3. Comparison between capturing different points on droplet, data from coated aluminum (5 mm) with a droplet volume of 44 µL (a) Position vs. time (b) Velocity vs. time

3. RESULTS AND DISCUSSION

Water droplet of different sizes are deposited on either uncoated or partially hydrophobic coated vertical aluminum surfaces, and volume of deposited droplet is increased during the progression of experiment on a tested surface, with an increment of 1 µL each time. Images captured during experiment show four different scenarios: 1) droplet remains stationary at deposition location, 2) droplet slides down to the edge/wettability gradient and pins at the location without visible further movements, 3) droplet slides down to the edge/wettability gradient and pins at the location, droplet oscillations are observed afterwards, 4) droplet detaches from sample after some droplet deformation is observed at the edge/wettability gradient.

On partially hydrophobic coated surfaces, advancing contact line of water droplets pin at positions near the wettability gradient, where slightly pass the boundary line, as shown in figure 4.

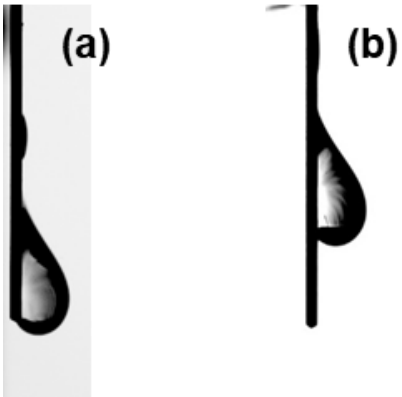

Figure 4. Pinned droplets on different sample surfaces (a) uncoated aluminum; (b) partially hydrophobic coated aluminum (5 mm)

Table 3 shows droplet size ranges for observing each scenario on all tested sample surfaces. The main discrepancy between different tested surface is the droplet size lower bound for scenario 4, which is the threshold for droplet detachment from the surface. On uncoated aluminum surface, the threshold is the highest, which a droplet volume of 55 µL is needed for droplet to detach. When hydrophobic coating is applied at the tip of the sample (1 and 2 mm coating region), the critical volume for droplet detachment is greatly reduced to 42 µL, showing that water drainage is improved on these samples. However, when the coating is applied on larger region at the end of sample, the critical volume for detachment goes back up to 51 µL, which only small improvement on drainage is achieved.

Table 3. Droplet size range for each scenario

	Uncoated	Coated (1 mm)	Coated (2 mm)	Coated (5 mm)
Remain stationary	≤ 28 µL	≤ 26 µL	≤ 28 µL	≤ 28 µL
Slide down, pinning without oscillation	29 - 36 µL	28 - 30 µL	29 - 33 µL	30 - 34 µL
Slide down, oscillate after pinning	37 - 54 µL	32 - 41 µL	34 - 41 µL	36 - 50 µL
Detach after sliding down	≥ 55 µL	≥ 42 µL	≥ 42 µL	≥ 51 µL

3.1 Initiation of Droplet Sliding

As droplet size ranges for each scenario shows, for all tested surfaces, the upper limits of droplet volume for observing scenario 1 are roughly the same. The reason behind this result is that droplet deposition locations are all on uncoated aluminum region for the tested surfaces. When volume of the deposited water droplet is below a certain volume, droplet sliding will not take place because a force balance between gravity and capillary force is achieved on the droplet, shown as

$$F_g = F_{capillary} \tag{1}$$

For surface at an inclination angle α

$$F_g = mg\sin\alpha \tag{2}$$

As for the capillary force, which holds the static droplet from starting to move, can be relate to the contact angles and surface tension by

$$F_{capillary} = k\gamma_{LV}R(\cos\theta_{re} - \cos\theta_{ad}) \tag{3}$$

where k is a constant, γ_{LV} is the liquid-vapor surface tension, R is the equivalent base radius of droplet contour, θ_{re} and θ_{ad} are receding and advancing contact angle of the droplet. As shown in figure 5., receding and advancing contact angle can be directly measured from images. By putting up all known values and measured droplet width together, calculations can be done to obtain an estimated value for k.

Value of retentive-force factor k obtained from experiment is then compared to those of existing droplet retention models, as shown in figure 6. The experiment result is found to be closest to results from Extrand & Kumagai. However, for model from Extrand & Kumagai, as well as the other one from ElSherbini & Jacobi, k would increase for contour aspect ratio that is larger than 1, which is very likely to be true in this experiment. Therefore, it is not proper to conclude which existing model gives best explanation to the experiment results. However, the experimental k clearly falls within the range of the various models, proving that the models apply well to this case.

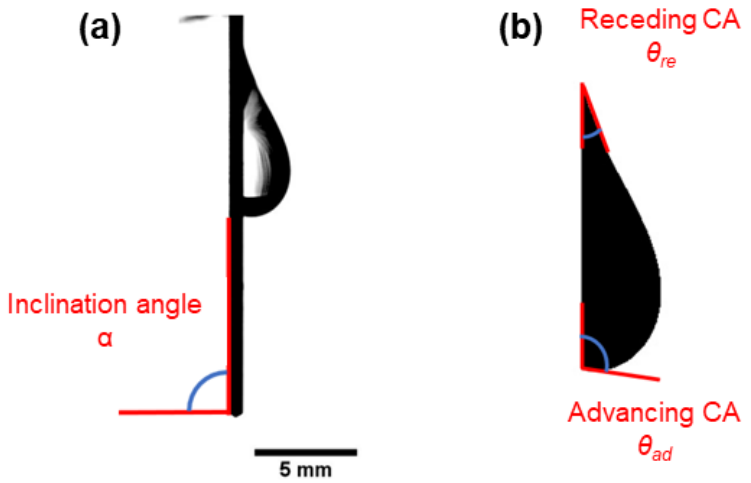

Figure 5. Critical static droplet at 28 µL (a) experiment image; (b) processed image for contact angle measurement

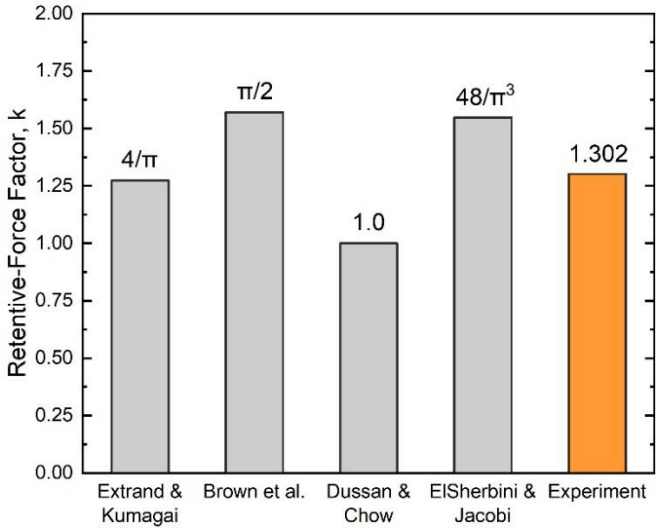

Figure 6. Retentive-force factor from experiment results, compared to earlier studies which disagreed upon assumptions for contact angles or contours

3.2 Droplet sliding process on uniform vertical surface

If size of deposited droplet exceeds the critical volume of it on the specific surface, droplet sliding will be initiated immediately after the deposition. The droplet undergoes acceleration until reaching either the edge (for uncoated sample) or wettability gradient (for partially coated sample) of the surface. Through observation in the experiments, it is found that the kinetic energy gained by droplet during sliding process will contribute to the droplet deformation after pinning, therefore maximum velocity reached by the droplet becomes one of the determining factors in droplet retention.

Figure 7 shows that maximum droplet velocities increase with droplet size at low droplet volumes, but the maximum velocity stops to increase at around 42 µL, thereafter, the maximum velocity decreases with droplet size.

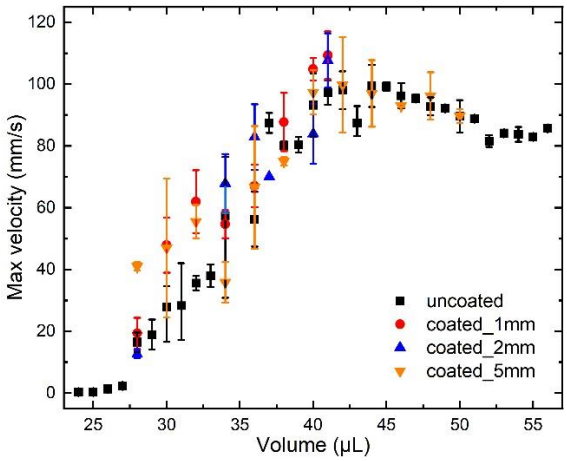

Figure 7. Maximum velocity vs. droplet volume

Figure 8 and 9 shows evolution of droplet velocity and acceleration throughout the experiment. Since experiments on uncoated surface covers a wider range of droplet size, examples are picked from uncoated sample. Firstly, since droplet sliding distances are the same, droplet sliding process will last shorter in sets of experiment in which droplet slide at higher velocity. As previously shown in figure 7, 40 µL droplet achieves a higher maximum velocity than 32 µL and 50 µL droplets. In every set of experiment, there is always a period when velocity gradient is significantly off the trend, and acceleration curve is showing a flat line at unreasonable value. This indicates an unstable droplet status caused by droplet deposition impact and is a major limitation in current experiment setup. While disregarding the "unstable" region in each curve, 40 µL droplet has the higher acceleration, which corresponds to its higher maximum

velocity. Another important trend in acceleration is that droplet acceleration decreases during the droplet sliding process. This trend is more obvious in 32 µL, where droplet acceleration gradually decreased from 197 mm/s^2 to 3 mm/s^2. The decrease in droplet acceleration can also be seen in 40 µL and 50 µL curve, though droplet instability and short sliding time make the trend unclear.

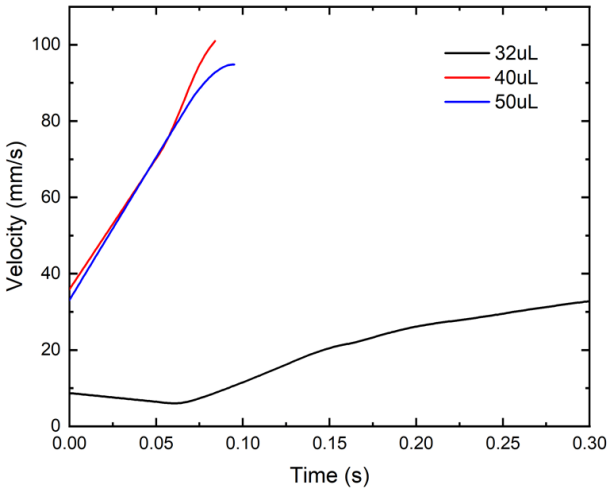

Figure 8. Droplet velocity vs. time, data from uncoated sample

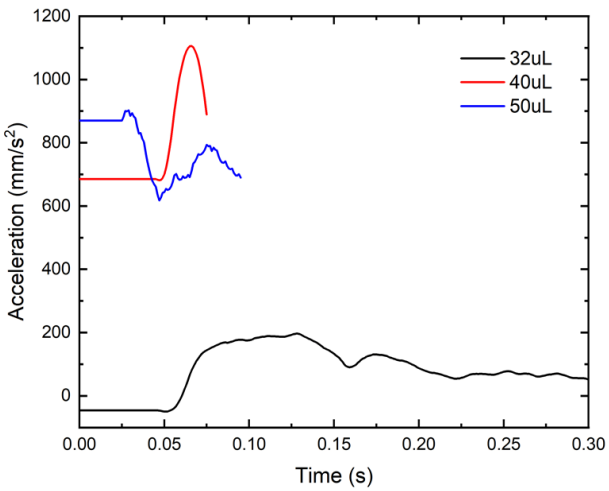

Figure 9. Droplet acceleration vs. time, data from uncoated sample

During droplet sliding distance, the resultant force acting on droplet is given by

$$F_R = ma = F_g - F_{capillary} - F_{vis} \tag{4}$$

In this equation, while F_g is easily obtainable since it is determined by droplet volume, capillary force $F_{capillary}$ and viscous force F_{vis} will be changing throughout droplet sliding, contributing to the variation of droplet acceleration in this process. In this case, F_{vis} will be determined by liquid viscosity, droplet volume, and sliding velocity, either of these factors will have a positive impact on F_{vis}, which acts against the motion of droplet. On the other hand, $F_{capillary}$, similar to previous section, is given by

$$F_{capillary,slide} = k_{slide}\gamma_{LV}R(\cos\theta_{re} - \cos\theta_{ad}) \tag{5}$$

Notice that k_{slide} is not equal to k from previous section, which is exclusively for static droplet. During droplet sliding process, both contact angles and droplet contour will be different from static droplets. Even with real time measurements of advancing and receding contact angles, capillary force on droplet can only be roughly estimated based on some assumptions to droplet contour. If sliding on hydrophilic surface, experiments show that droplet contour change periodically, which adds even more complicity to the calculation.

In this work, experiments also reproduced part of a phenomenon found by Wang *et al.*. Figure 10 shows the advancing contact angle of droplet when the droplet is free of any instability caused by deposition process (at maximum velocity). Experiments in this work show that advancing contact angle of sliding droplet increase linearly with droplet velocity.

In addition to results from this work, Wang *et al.* also showed that receding contact angle decreases with droplet velocity. This finding suggests that contact angle hysteresis of a sliding droplet will increase as sliding velocity increases, therefore leading to an increase in the capillary force which acts against droplet motion.

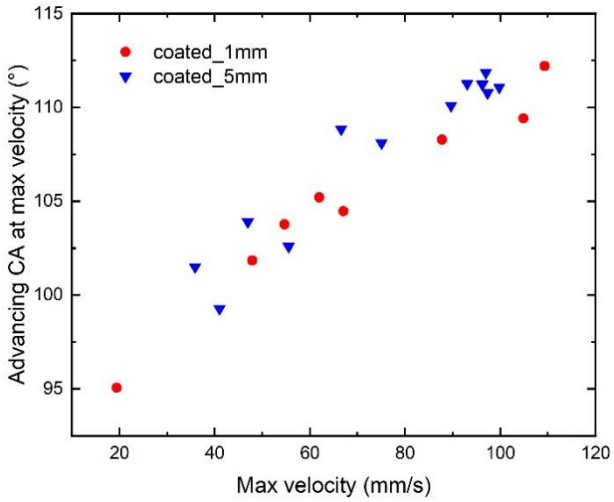

Figure 10. Advancing contact angle vs. droplet velocity

At the moment after initiation of droplet motion, sliding velocity does not have an impact on viscous force since droplet starts at zero velocity, thus liquid viscosity and droplet volume determines initial viscous force acting on the droplet. For the case in experiment, liquid viscosity remains unchanged throughout whole experiment, then initial viscous force increases as droplet volume increases. As the droplet accelerates down the surface, higher velocity leads to increase in both viscous force and contact angle hysteresis, which also gives rise to increased capillary force, and further reduce the resultant force on the droplet. Due to the limitation of sliding distance, droplets at majority of the tested volumes do not reach their stable sliding velocities, which droplet acceleration reduces to zero, and droplet velocity remains at its maximum value. Therefore, all measured maximum velocities at high droplet sizes are under collective effects from different droplet mass, initial acceleration, reduction of acceleration during sliding, and limitation of sliding distance. In the tested situation, when droplet size exceeds 42 µL, maximum droplet velocity no longer increases with droplet size, and starts to decrease instead.

3.3 Droplet oscillation after pinning

After water droplet pinning at either the sample edge or wettability gradient, oscillations are observed from experiment trials where droplet size is large enough and carries sufficient momentum. For clearer analysis on the droplet oscillations, a reference position is introduced to data processing of this part. For uncoated experiment, the y-position of sample edge is the reference position; for coated experiments, the y-position of the boundary is the reference position. The reference position will be set as zero, and positive direction points downwards. This helps to analyze how droplet equilibrium position evolve with increasing droplet volume.

Figure 11 shows that droplet equilibrium position grows as droplet volume increases. It can also be found that equilibrium position increases at higher rate on coated surfaces than on uncoated surface. The main reason to this phenomenon is that droplets on coated samples do not pin exactly at the wettability gradient line. Figure 13 shows that the advancing contact line moves below gradient line, and the distance of this movement depends on droplet size.

With clear identification of droplet equilibrium position on its pinning location, maximum deformation experienced by the droplet can be quantified as first peak amplitude in position-time plot. Figure 12 shows how first peak amplitude evolves with increasing droplet size. On coated samples, amplitude generally increases with droplet size until droplet size is large enough for it to detach from the sample. Also, it can be noticed that maximum amplitudes reached on three coated samples are identical, which probably means that droplet will detach from the sample if deformation exceeds a certain value.

On uncoated sample, unlike the coated ones, droplet can wet around the sample edge, and the advancing contact line will move to lower surface of the sample. Following this phenomenon, a slight horizontal displacement of the droplet center of mass is observed in data analysis. In figure 12, first peak amplitude on uncoated sample decreases at high droplet volume. This indicates that due to droplet wetting around sample edge, after a certain amount of droplet motion vertically downward, further deformation goes in horizontal direction instead.

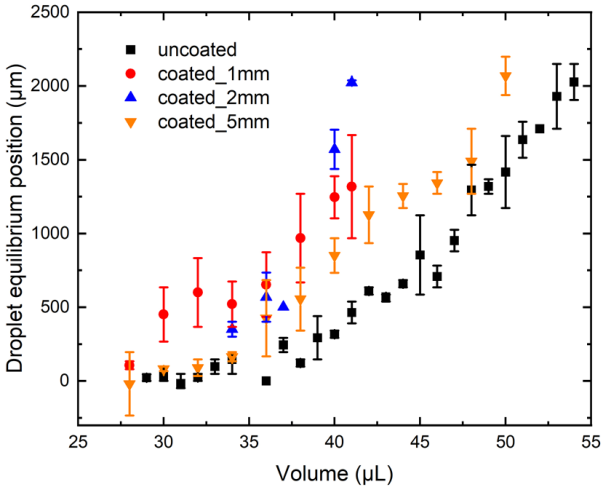

Figure 11. Droplet equilibrium position vs. droplet volume

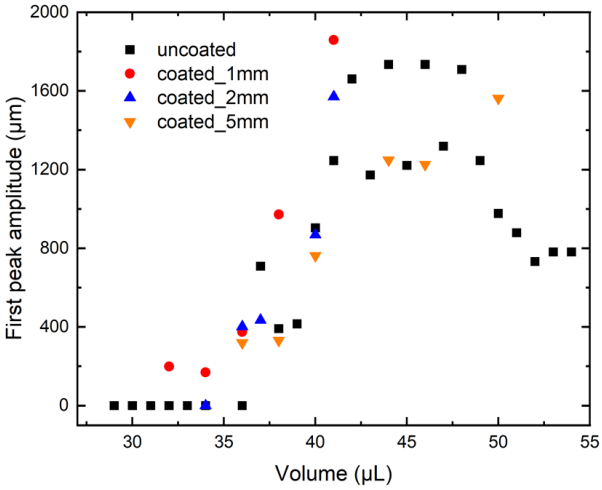

Figure 12. First peak amplitude vs. droplet volume

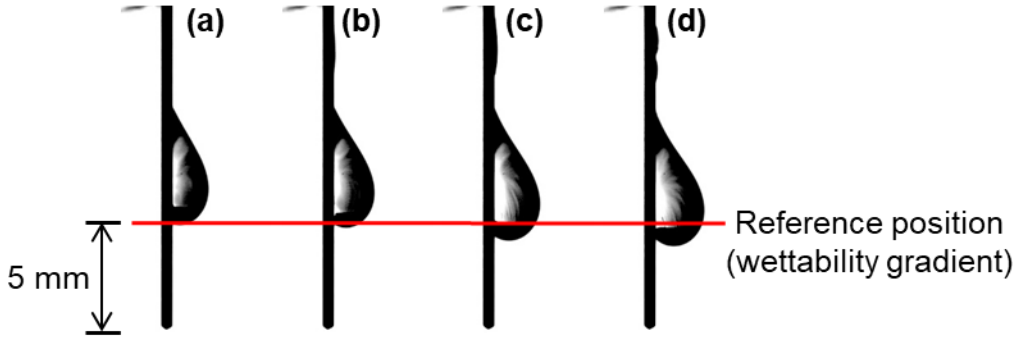

Figure 13. Comparison between equilibrium positions from different droplet volume (a) 28 μL (b) 34 μL (c) 40 μL (d) 46 μL

In addition to amplitude aspect of droplet oscillation, frequency can also be obtained through peak analysis. Figure 14 shows droplet oscillation frequency at different droplet sizes. The data points from four different samples generally share the same trend, which oscillation frequency decreases as droplet size increases.

Due to the resemblance of droplet oscillation to harmonic oscillator, here we assume the droplet oscillatory motion is a harmonic oscillator and carry out some preliminary analysis.

For a translational mechanical harmonic oscillator system, the natural frequency relates to object mass and spring constant by:

$$f = \frac{1}{2\pi}\sqrt{\frac{k}{m}} \tag{6}$$

where f is natural frequency of the system in Hz, k is spring constant in N/m, m is object mass in kg.

In this case, frequency of oscillation and droplet mass are both known. Therefore, we can obtain spring constant of the droplet oscillation, thus learn about the stiffness of droplet when it is being deformed after pinning. Figure 15 shows the results from such analysis. Results from four samples share the same decreasing trend, meaning that for all tested cases, droplets appear to be easier to deform when droplet volume is increased. This decrease in droplet stiffness is probably also a factor that contributes to the increase in first peak amplitude when droplet size increases.

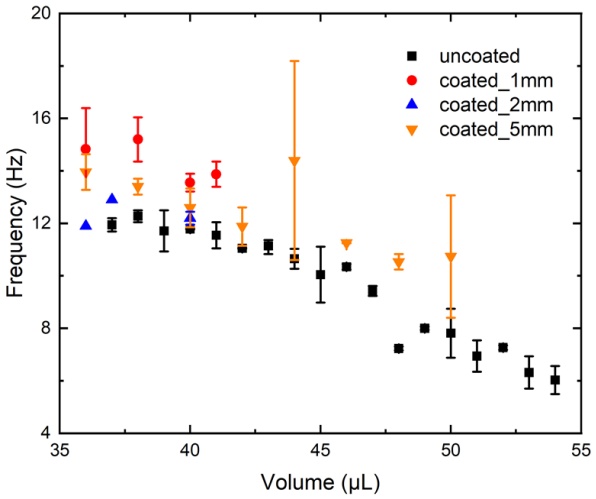

Figure 14. Droplet oscillation frequency vs. droplet volume

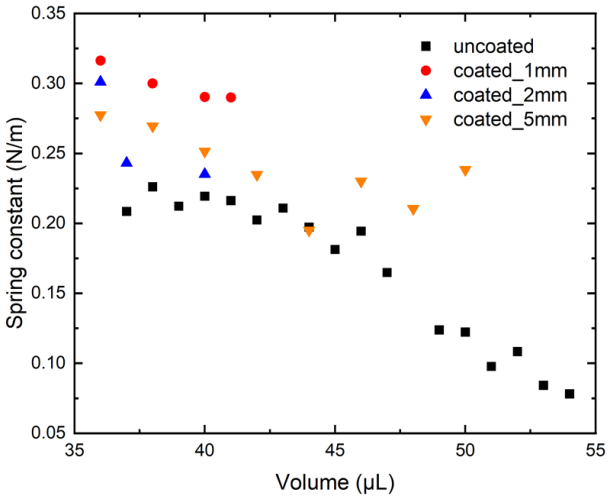

Figure 15. Oscillation spring constant vs. droplet volume

4. CONCLUSION

In this work, droplet motion after its deposition on a vertical surface is observed and recorded with a high-speed camera. Analysis on such process is conducted by respectively looking into initiation of droplet sliding, droplet sliding process, and oscillatory droplet deformation after pinning. In addition to typical aluminum surface that is widely used on heat exchangers in air-conditioning and refrigeration systems, three partially hydrophobic coated samples of different sized coating region are also tested. Conclusions from this work are summarized below:

- By preventing water droplet from wetting around the sample edge, partially hydrophobic coated samples reduce critical volume for droplets to detach, thus enhancing water drainage. However, the effect of this drainage enhancement depends upon length of coated region. On samples with 1 mm and 2 mm coated region at the tip, drainage is significantly improved, but only small enhancement is seen on sample with 5 mm coated region.
- Initiation of droplet sliding on vertical surface is determined by the balance between gravity and capillary force acting on the droplet. Constant k for estimating capillary force is calculated from experiment results and compared with existing models. Comparison shows that existing models give good estimations for capillary force, but still slightly off the exact value, probably due to some incompatibilities between real case and assumptions in model.
- During droplet sliding, resultant force acting on droplet decides upon gravity, capillary force, and viscous force. While gravity is fixed for specific droplet, capillary force increases as velocity increases due to change in contact angle hysteresis. Viscous force increases with increasing droplet volume and increases as velocity is increased. Maximum velocity reached by droplet before pinning is determined by these factors, along with limitation of sliding distance.
- Droplet deformation and oscillation after pinning is complicated. Droplet volume, velocity, type of energy barrier that causes pinning (edge/wettability gradient) all have impact on the first largest deformation (first peak) and following oscillations. This work illustrates some findings on droplet behavior after pinning and shows that droplet stiffness during such deformation decreases with droplet volume through experiment.

REFERENCES

Makkonen, L. (1984). Modeling of ice accretion on wires. Journal of Applied Meteorology and Climatology, 23(6), 929-939.

Hung, L. S., & Yao, S. C. (1999). Experimental investigation of the impaction of water droplets on cylindrical objects. International journal of multiphase flow, 25(8), 1545-1559.

Wang, S., & Desjardins, O. (2018). 3D numerical study of large-scale two-phase flows with contact lines and application to drop detachment from a horizontal fiber. International Journal of Multiphase Flow, 101, 35-46.

Tang, A. D., & Jacobi, A. M. (2001). Air-Side Heat Transfer with Highly Interrupted Surfaces: An Experimental Study of Condensate Retention Effects. Air Conditioning and Refrigeration Center. College of Engineering. University of Illinois at Urbana-Champaign.
Min, J., & Webb, R. L. (2001). Condensate formation and drainage on typical fin materials. Experimental Thermal and Fluid Science, 25(3-4), 101-111.
Korte, C. M., & Jacobi, A. M. (1997). Condensate retention and shedding effects on air-side heat exchanger performance. Air Conditioning and Refrigeration Center. College of Engineering. University of Illinois at Urbana-Champaign.
ElSherbini, A. I. (2003). Modeling condensate drops retained on the air-side of heat exchangers. University of Illinois at Urbana-Champaign.
ElSherbini, A. I., & Jacobi, A. M. (2004). Liquid drops on vertical and inclined surfaces: I. An experimental study of drop geometry. Journal of colloid and interface science, 273(2), 556-565.
ElSherbini, A. I., & Jacobi, A. M. (2004). Liquid drops on vertical and inclined surfaces: II. A method for approximating drop shapes. Journal of colloid and interface science, 273(2), 566-575.
ElSherbini, A. I., & Jacobi, A. M. (2006). Retention forces and contact angles for critical liquid drops on non-horizontal surfaces. Journal of colloid and interface science, 299(2), 841-849.
Kim, H. Y., Lee, H. J., & Kang, B. H. (2002). Sliding of liquid drops down an inclined solid surface. Journal of colloid and interface science, 247(2), 372-380.
X. Wang, L. Wang, R. Yu, 2016, Dynamic Contact Angle on Surface with Gradient in Wettability
Extrand, C. W., & Kumara, Y. (1995). Liquid drops on an inclined plane: the relation between contact angles, drop shape, and retentive force. Journal of colloid and interface science, 170(2), 515-521.
Brown, R. A., Orr Jr, F. M., & Scriven, L. E. (1980). Static drop on an inclined plate: analysis by the finite element method. Journal of Colloid and Interface Science, 73(1), 76-87.
Chow, R. T. P. (1983). On the ability of drops or bubbles to stick to non-horizontal surfaces of solids. Journal of Fluid Mechanics, 137, 1-29.

ACKNOWLEDGEMENT

The authors are grateful to the financial support from the Air Conditioning and Refrigeration Center at the University of Illinois at Urbana-Champaign.